Journal of Hazardous Materials 205–206 (2012) 63–71

Contents lists available at SciVerse ScienceDirect

Journal of Hazardous Materials

journal homepage: www.elsevier.com/locate/jhazmat

In vitro biodurability of the product of thermal transformation of cement–asbestos

Alessandro F. Gualtieri[a,*], Alberto Viani[a], Giulia Sgarbi[a], Gigliola Lusvardi[b]

[a] *Dipartimento di Scienze della Terra, Università di Modena e Reggio Emilia, Via S. Eufemia 19, I-41100 Modena, Italy*
[b] *Dipartimento di Chimica, Università di Modena e Reggio Emilia, Via G. Campi 183, I-41100 Modena, Italy*

ARTICLE INFO

Article history:
Received 8 September 2011
Received in revised form 1 December 2011
Accepted 2 December 2011
Available online 13 December 2011

Keywords:
Cement–asbestos
Recycling
Dissolution
Biodurability *in vitro*
Rietveld method
SEM

ABSTRACT

To safely recycle the product of the thermal transformation of cement–asbestos as secondary raw material, its toxicity potential should be assessed by *in vitro* biodurability tests. In this work, the acellular *in vitro* biodurability of the products of transformation of cement–asbestos at 1200 °C (named KRY·AS) was tested using both inorganic and organic simulated lung fluids at pH 4.5. The dissolution kinetics were followed using chemical, mineralogical and microstructural analyses. The total dissolution time estimated from the experiments with inorganic HCl diluted solution is one order of magnitude higher than that determined from the experiments with buffered Gamble solution (253 days *vs.* 20 days). The key parameter determining the difference in dissolution rate turns out to be the solidus/liquidus ratio which prompts a fast saturation of the solution with monosilicic acid. The calculated dissolution rate constants showed that the biodurability *in vitro* of KRY·AS is much lower with respect to that of standard chrysotile asbestos (total estimated dissolution time of 20 days *vs.* 298 days, respectively). This proves a low potential toxicity of this secondary raw material.

1. Introduction

According to the recent European directives, the need for environmentally friendly alternative solutions to landfill disposal prompts the recycling of hazardous wastes as secondary raw materials. Disposal of hazardous wastes such as asbestos-containing materials (ACM) has become a matter of concern in European countries [1]. For example, cement–asbestos slates in open environment have to be removed sooner or later as their degradation may prompt release of breathable airborne fibres [2,3]. The awareness of the health-threat of asbestos has prompted policy of abatement and disposal of ACM. However, disposal of cement–asbestos in controlled landfills does not seem to be the ultimate solution because zero risk of fibre dispersion in air and water cannot be guaranteed. An alternative solution is the thermal transformation of ACM into non-hazardous products and their safe recycling as secondary raw material [4–10]. Along this line, an industrial process for the thermal destruction of asbestos containing wastes was recently developed [11]. Sealed packages of cement–asbestos slates undergo prolonged annealing at a temperature in the range 1200-1300 °C, during which both serpentine and amphibole asbestos minerals are transformed into newly formed silicate phases [12,13].

The secondary raw material produced after the thermal treatment at 1200 °C, named KRY·AS, is mainly composed of SiO_2 and CaO with minor MgO, Al_2O_3, and Fe_2O_3. Its chemical and mineralogical nature is similar to that of a Mg-rich clinker. Having reassured the reliability of the novel industrial process, suitable and attractive recycling solutions were successfully explored [11,14]. To safely reuse KRY·AS, its toxicity must also be tested. One of the parameters commonly used to evaluate the potential toxicity of mineral fibres/particles is biodurability, that is the *biopersistence* of a fibre in human lung fluids or the resistance of a fibre to dissolution over a lifetime [15]. Besides that, *in vitro* tests in cell cultures for the determination of the cyto/geno-toxicity and *in vivo* tests on rats/mices for the determination of the cancerogenicity are generally carried out. The cytotoxicity of thermally treated cement–asbestos and a commercial Mg-rich clinker has recently been tested *in vitro* in cellular cultures [16]. It was found that cytotoxic cell damage of more extended grade is exerted by the untreated cement–asbestos compared to the thermally treated material KRY·AS. The activity of thermally treated cement–asbestos is similar to that of the negative control clinker cement as regards cell growth rate and viability. These results are very promising for a safe recycling of KRY·AS in different industrial applications but need further confirmation. To this aim, in this work the acellular biodurability of KRY·AS is tested *in vitro* using simulated lung fluids which reproduce the acid chemical environment of macrophages.

In the past, the study of acellular biodurability of asbestos fibres has been attempted mainly using two approaches whose major

* Corresponding author. Tel.: +39 059 2055810; fax: +39 059 2055887.
E-mail address: alessandro.gualtieri@unimore.it (A.F. Gualtieri).

0304-3894/$ – see front matter © 2011 Elsevier B.V. All rights reserved.
doi:10.1016/j.jhazmat.2011.12.005

difference is the nature of the dissolving solution: hydrochloric *vs.* modified organic Gamble solution. These study cases are only a limited set of many papers reported in the literature dealing with asbestos dissolution in inorganic and organic solutions mimicking lung conditions to evaluate biopersistence of asbestos fibres. The assessment of the acellular biodurability should also be compared with the results of *in vivo* studies where dissolution of asbestos fibres is monitored directly in the lungs of laboratory animals (mices, rats, etc.).

The "hydrochloric solution" approach has been used in the experiments conducted by Hume and Rimstidt [17] who estimated the dissolution time of breathable-size chrysotile fibres. The fibre size considered most hazardous to the lung tissue has a diameter of less than 1 μm and is longer than 10 μm [18]. Hume and Rimstidt [17] found that the dissolution rate of chrysotile in simulated organic media (pH 2.0–6.0) is a two-step reaction: first, the magnesium hydroxide layer of the chrysotile dissolves, leaving behind silica that dissolves later. The latter is the rate limiting step of the reaction. In that paper, the authors also predicted that a fibre of chrysotile of 1 μm in diameter will completely dissolve in about 9 months. Different results were found by Bernstein et al. [19–21] who investigated the dynamics and rate of clearance of chrysotile in a biopersistence study *in vivo*. In those studies, clearance times of the order of days were reported: chrysotile fibres longer than 20 μm were cleared with a half-time of 1.3 days, most likely by dissolution and breakage into shorter fibres. Shorter fibres were also rapidly cleared from the lung with fibres 5–20 μm clearing even more rapidly (half-time of 2.4 days) than those with length lower than 5 μm (half-time of 23 days). Breaking of the longer fibres is expected to increase the short fibre pool and therefore could account for this difference in clearance rates.

In the "Gamble solution" approach, Oze and Solt [22] compared dissolution rates up to 720 h at pHs 1.2 and 7.4 for chrysotile and tremolite asbestos in contact with a modified Gamble solution, finding that bulk mineral–solution interactions govern mineral dissolution. Batch dissolution experiments were performed at body temperature (37 °C) to examine asbestos biodurabilities in a slightly salty, acid digestive fluid (simulated gastric fluid SGF) compared to the higher ionic strength, near-neutral pH lung fluid (simulated lung fluid SLF). The estimated lifetime of fibres with 1 μm diameter and 10 μm length was: 1 day for chrysotile and 274 days for tremolite in SGF, respectively; 583 days for chrysotile and 1452 days for tremolite in SLF, respectively.

Because different dissolution rates are expected using the two different approaches, in this project two experimental lines were arranged. Following the experimental conditions reported in [17], in one experimental line solid phases were put in contact with an hydrochloric acid solution whereas following the experimental conditions reported in [22], in a second experimental line, solid phases were put in contact with a modified Gable solution. In the latter experiment, chrysotile asbestos was tested in parallel with KRY·AS as a reference.

De Meringo et al. [23] report that no standardization of the methodology for acellular *in vitro* assessment of biodurability has appeared so far, and the main differences among all the applied methods concern the type of fluid used, the morphology of the test material, and the type of test, whether static or dynamic.

2. Experimental

2.1. The investigated samples

The secondary raw material (KRY·AS) used for these experiments is described in [11,14]. It was prepared by the industrial thermal treatment of standard sealed packs of cement–asbestos slates removed from industrial sites. The packs were placed in a discontinuous industrial kiln and exposed to a firing cycle of 40 h, including a 21 h long isothermal step at 1200 °C [11]. Chemical composition as well as mineralogical assemblage of the slates were shown to be strongly dependent upon the production plant [24]. As a consequence, packs of slates coming from different plants that underwent the same thermal treatment, yielded KRY·AS with different phase composition. On the basis of the available data, KRY·AS can be roughly sorted out in two classes: one with a prevailing amount of β-larnite (C2S, Ca_2SiO_4), and one containing akermanite ($Ca_2MgSi_2O_7$) as major phase. These major phases are invariably accompanied by other Al-, Ca-, Mg-rich silicates, common components of Mg-rich clinkers, and amorphous phase. Samples 1 and 2 are representative of the C2S-rich class whereas Sample 3 is representative of the akermanite-rich class.

Sample 4 is standard chrysotile asbestos SRM1866A provided by the National Institute of Standard Technology (NIST) used for comparison in the dissolution experiments with organic simulated lung fluids. Besides clino-chrysotile, Sample 4 contains magnetite as minor impurity. The specific surface of this sample measured with the BET (Brunauer–Emmett–Teller) method is 51.7 m^2/g. Further details of the sample can be found in Cattaneo et al. [12]. Chrysotile was chosen as control in dissolution tests instead of cement–asbestos in the attempt to compare its biodurability with that of KRY·AS and assess whether the latter has a lower biodurability than the dominant toxic asbestos fibres of cement–asbestos. Crocidolite, amosite or tremolite possibly found in cement–asbestos mixtures could also have been selected as positive controls but the dissolution rate of these minerals, as reported in the literature, is so low that in the time spam of our experiments, no reaction would have been recorded. One limit in the use of chrysotile as positive control with respect to cement–asbestos is that the dissolution process of KRY·AS from the chemical and mineralogical point of view would have been better compared to that of the original cementitious matrix cement–asbestos.

The mineralogical and X-ray fluorescence (XRF) chemical compositions of the samples are shown in Table 1. The table also reports loss of ignition, BET specific surface and parameters related to the grain size distribution determined using laser granulometry (D10 = the sediment size (in μm) for which 10% of the sediment sample is finer, D50 = Mass-median-diameter (MMD): the sediment size for which 50% of the sediment sample is finer, D90 = the sediment size for which 90% of the sediment sample is finer).

2.2. The experimental lines

Two lines of experiments with different parameters were arranged. The parameters that were kept fixed in both lines are the nature of the material, starting pH (4.5) value, static mode, and temperature. In the first experimental line, dissolution was followed in hydrochloric acid solution with external buffering of the solution, no stirring/agitation, and a ratio between the solidus (mg) and liquidus (ml) of 0.67. In the second experimental line, dissolution was followed in a modified Gamble solution, with constant agitation of the suspension and a ratio between the solidus (mg) and liquidus (ml) of 0.2. In both lines, the determination of the biodurability was determined with *in vitro* acellular dissolution experiments reproducing the chemical environment of the macrophage cells (pH 4.5).

In the first experimental line, the simulated lung fluid was prepared using only hydrochloric acid (HCl). The C2S-rich KRY·AS Sample 1 was tested in this experimental line. Parallel medium-short term tests have been conducted using the other akermanite rich KRY·AS Sample 3 showing a very similar dissolution behaviour of Sample 1. For this reason, the long-term dissolution experiment was conducted to the end only for Sample 1. The experimental line was arranged with a batch of 15 aliquots at room temperature and

Table 1
The mineralogical, chemical and physical characterization of the investigated samples. Sample 1, 2, 3. Data relatively to Sample 4 are reported in the text and in [11].

	Sample 1	Sample 2	Sample 3
Rietveld agreement factors, as defined in [27]			
R_{wp} (%)	6.60	5.62	6.73
R_p (%)	5.15	4.12	4.89
χ^2	1.43	3.42	6.15
Phase	wt%	wt%	wt%
Akermanite	1.0(3)	–	55.0(1)
Bredigite	–	–	7.3(2)
Calcite	–	–	0.6(1)
C2S	71.2(2)	67.3(1)	4.9(2)
C3A	–	–	0.5(1)
Ferrite	4.8(3)	6.5(2)	–
Magnetite	–	–	0.5(1)
Merwinite	7.5(4)	1.8(1)	8.9(2)
Periclase	8.7(2)	6.3(1)	–
Portlandite	–	4.2(2)	–
Quartz	–	–	1.8(1)
Ternesite	–	4.3(1)	–
Wollastonite	–	1.1(1)	2.9(1)
Yeelimite	–	0.4(1)	–
Amorphous	6.8(1.0)	8.1(4)	17.6(5)
BET (m2/g)	1.2	1.6	2.7
D10 (μm)	1.1	4.3	1.3
D50 (μm)	6.5	12.6	5.7
D90 (μm)	39.9	52.5	17.4
Oxides	wt%	wt%	wt%
SiO_2	30.8	23.0	36.8
Al_2O_3	5.4	3.97	6.59
Fe_2O_3	3.8	2.54	4.36
TiO_2	0.28	0.21	0.27
CaO	48.5	55.3	40.1
MgO	7.5	7.34	8.28
Na_2O	0.36	0.12	0.7
K_2O	0.34	0.36	0.35
SO_3	1.59	2.15	0.30
Loss of ignition	1.43	4.59	1.82

a batch of 4 individuals at 37 °C to reproduce the body temperature. For each treatment, 0.1 g of powder sample was poured in a glass bottle together with 150 ml hydrochloric acid solution with pH 4.5. The experimental mode was static and the bottles containing the suspension were shaken vigorously once a day. To monitor the complete reaction kinetics at pH 4.5, individuals were sampled at selected time intervals well above the virtual completion of the reaction. For the experiment line at 25 °C, the sampling schedule was: 1 = 6 h, 2 = 1 day, 3 = 2 days, 4 = 7 days, 5 = 14 days; 6 = 28 days; 7 = 60 days; 8 = 90 days; 9 = 120 days; 10 = 180 days; 11 = 210 days; 12 = 270 days; 13 = 365 days; 14 = 481 days; 15 = 561 days. For the experimental line at 37 °C, the sampling schedule was: Sample 1b = 6 h, Sample 2b = 1 day, Sample 3b = 2 days, Sample 4b = 7 days.

After sampling, the suspension was filtered, weighted and dried for the successive analytical step. During the experiment, the reaction between the solid phase and liquid brings new ionic species in solution. Hence, besides ion activity in solution, the pH of the solution gradually increases with time in absence of any buffer. Thus, after each sampling, pH was corrected to 4.5 with the addition of HCl (external pH buffering). The measure of pH was performed using a 3310 JENWAY instrument which was calibrated using 2 standard solutions at pH 4.0 and 7.0.

In the second experimental line, the C2S rich KRY·AS Samples 2 and 3 were tested together with standard chrysotile. Following Oze and Solt [22], a batch of modified Gamble solution buffered at pH 4.5 was used for this experimental line. Several replicates of samples were simultaneously brought in contact with a fixed volume of Gamble solution in polypropylene sample vials and kept at 37 °C (static mode) under continuous agitation using an oscillating bottle holder system inside the low temperature kiln. To select a liquidus/solidus ratio high enough to reduce the need for external pH corrections, 50 mg of sample and 250 ml of solution were prepared. At least 9 sample replicates were prepared and tested at increasing time intervals. The sampling schedule for Samples 2 and 4 can be summarized as follows: replicate 1 = 4 h, 2 = 6.5 h, 3 = 12 h, 4 = 25 h, 5 = 60 h; 6 = 120 h; 7 = 171 h; 8 = 337 h; 9 = 480.5 h. For Sample 3: replicate 1 = 6.5 h; 2 = 12.5 h; 3 = 24.5 h; 4 = 49 h; 5 = 97.5 h; 6 = 170.5 h; 7 = 292 h; 8 = 341 h; 9 = 532 h.

At the end of each time period, the pH of the fluid was measured and the solid was separated from the solution *via* filtration. The solid was then collected from a platinum crucible after calcination to remove the filter paper.

2.3. Analytical methods

The following analyses were conducted:

Determination of the relative weight loss of the residue, indicative of the advancement of the dissolution process (in triplicate). 2.5 μm filters which were previously conditioned and weighed were used for filtration. The filter + residues aggregate was dried at 105 °C for 1 h and weighed again to determine the weight of the residue. To cross-check the result, the filter + residues were calcined in Pt crucible at *ca.* 800 °C to separate the solid fraction to be weighed.

Determination of the element concentration (aluminium, calcium, iron, magnesium, and silicon) in the filtered solution after filtration. Calcium and magnesium were determined with atomic absorption spectroscopy using an AAnalyst 100 Perkin Elmer. Aluminium, iron, and silicon were determined with ICP–OES (Inductive Coupled Plasma–Optical Emission Spectrometry) instrument Optima 4200 DV Perkin Elmer.

Mineralogical quantitative phase analyses to follow the dissolution of the crystalline and amorphous phases composing KRY·AS in the acid simulated inorganic environment were conducted using X-ray powder diffraction (XRPD). Data were collected using a Bragg–Brentano θ–θ diffractometer (PANalytical, Cu Kα radiation, 40 kV and 40 mA) equipped with a real time multiple strip (RTMS) detector. Divergence and anti-scattering slits of 0.125° and 0.25°, respectively, were mounted in the incident beam pathway. The pathway of the diffracted beam included a Ni filter, a soller slit (0.02 rad) and antiscatter blade (5 mm). The virtual step scan of the measurement was 0.0167°2θ. Due to the paucity of the sample powders, a silicon zero background sample holder was used. The quantitative phase analyses were performed using the Rietveld method [25]. The refinements were accomplished with the GSAS [26] package and its graphical interface EXPGUI [27]. The determination of both crystalline and amorphous content was calculated using the combined Rietveld–RIR method [28]. The calculated weight estimates were normalized with respect to the weight of the solid fraction and expressed in mg.

Scanning electron microscopy (SEM) study of the residual dissolution products was conducted using a Philips XL-40 instrument equipped with an energy dispersive X-ray fluorescence spectrometer (EDS). For the observations, a tiny amount of each sample powder was loaded on an aluminium stub and Gold coated.

3. Results and discussion

3.1. Dissolution in inorganic simulated lung fluids

Fig. 1 reports the variations of pH of the suspension and weight of the residual fraction of KRY·AS with time. Both pH (stable at a value of 4.5) and weight loss reach a plateau after about 300 days indicating that the chemical reaction is completed.

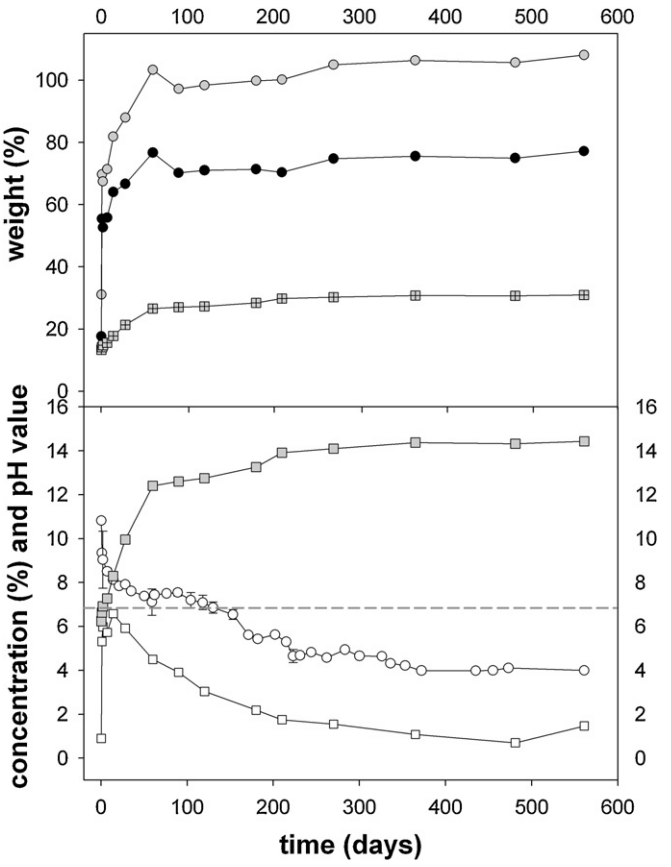

Fig. 1. Time evolution of pH of the suspension and weight of the residual fraction of KRY·AS with respect to silica. See the text for details. Legend: empty dots = pH; empty squares = Si^{4+} in solution (concentration % with respect to the total amount of Si^{4+} contained in KRY·AS); grey squares = rescaled Si^{4+} in solution (concentration % with respect to the total amount of Si^{4+} contained in KRY·AS); black dots = raw weight loss; grey squares = rescaled (amorphous) silica determined from the value of the rescaled fraction of Si^{4+}; grey dots = total rescaled weight loss (raw weight loss plus precipitated silica). Because, a fraction of the amorphous phase is also due to silica re-precipitated from the solution, the chemical composition of the residue and the additional silicon precipitated from the solution and concentrated in the solid phase were determined. This value has been summed up to the Si^{4+} measured in solution to yield a graph of the "rescaled" Si^{4+} and corresponding "rescaled" amorphous SiO_2. If such extra silica is added to the calculated raw weight loss, the actual "rescaled" weight loss during KRY·AS dissolution is obtained.

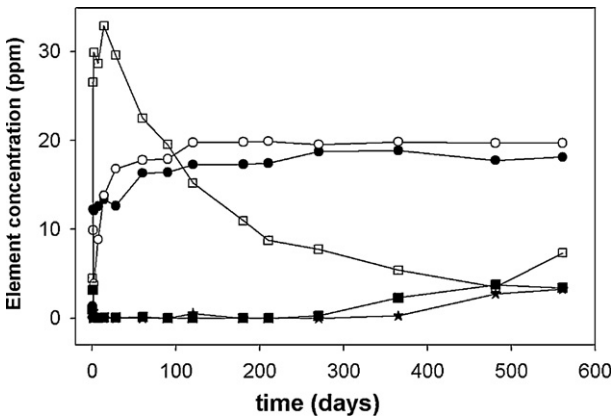

Fig. 2. Release in solution of the major elements contained in KRY·AS (line 1, Sample 1) during the dissolution experiment. For sake of clarity some values have been multiplied by a rescaling factor indicated in the legend. Legend: Black dots = Ca^{2+} ppm/10; Empty dots = Mg^{2+}; Empty squares = Si^{4+}; Black stars = Fe^{3+} ppm × 5; black squares = Al^{3+}.

As shown later, the apparent incomplete dissolution of the solid fraction is due to the precipitation of secondary silica from the Si-supersaturated solution. There is no appreciable difference between the experiments conducted at room temperature and 37 °C (see Supplementary data Fig. S1), since weight loss and pH values at 37 °C and 25 °C are almost identical.

Fig. 2 and Supplementary data Table S1 report the data relative to the release in solution of the major elements constituting KRY·AS. The dissolution of the Si-rich original phases promotes the release of Si in solution which in turn precipitates as silica aggregates. Magnesium is completely released in about 100 days whereas calcium is totally released in about 300 days. The release of aluminium and iron is fairly different as it starts after about 250–300 days and ends after about 350–400 days.

A gallery of SEM micrographs of the KRY·AS residue during the dissolution experiment at pH 4.5 is portrayed in Supplementary data Fig. S2. The SEM study shows that after 6 h, rare relics of transformed asbestos fibres visible due to the phenomenon of pseudo-morphosis extensively described in Gualtieri et al. [11] are still observed. After 7 days, the observed specimen revealed the presence of idiomorphic calcite crystals precipitated from the solution likely as a consequence of a temporary Ca-oversaturation of the system after Ca-rich silicates dissolution. Calcite precipitation continues and shows a maximum rate after *ca.* 28 days. Aggregates of micrometric grains of cement crystalline phases and likely amorphous phase are shown in an image representative of the experiment after 28 days. The average grain size of the reacting grains is significantly reduced after 180 days in contact with the acid solution. The residue after 365 and 481 days is composed of silica particle aggregates with minor iron and aluminium, as confirmed by the EDS analysis.

The Rietveld phase composition of the residues of the dissolution process is reported in Supplementary data Table S2. Fig. 3 reports the actual weight of each crystalline phase normalized with respect to the weight of the solid fraction in mg. The dissolution trends can only be understood if the evolution of the weights is compared to the trend of ions release in solution.

C2S, the major phase of the system, is the first crystalline phase to dissolve. Its fraction is close to zero after about 14 days (see Fig. 3a and Supplementary data Table S2).

Crystallization of calcite and portlandite, simultaneous to C2S dissolution is observed here and is responsible for the increase of pH after about 100 days (see Fig. 1). Both calcite and portlandite are metastable and completely dissolve after *ca.* 120 days (Fig. 3a). The comparison of the concentration of Ca^{2+} released in solution with time in Fig. 2 and the evolution of the Ca-bearing crystalline phases in Fig. 3 reveals that most of Ca^{2+} is liberated during the decomposition of C2S with a first minor plateau in the range 14–28 days in correspondence with the precipitation of portlandite and calcite. Portlandite ($Ca(OH)_2$) and/or calcite ($CaCO_3$) are also observed as secondary products during the acid dissolution of Portland cements [29].

The dissolution of the crystalline phases is a two-step process which involves amorphization of the crystalline network and successive dissolution. The formation of intermediate amorphous phase is witnessed by the increase of the amorphous fraction (black dots in Fig. 3a) whenever decomposition of a crystalline phase occurs. A significant fraction of the amorphous phase is also due to silica precipitated back from the oversaturated solution (see Fig. 1). In fact, silicon is the other element released during the decomposition of C2S. Figs. 1 and 2 show a striking decline of Si released in solution with time which is effective when pH < 6.5. We have determined the chemical composition of the residue and calculated the additional silicon precipitated from the solution and concentrated in the solid phase. This value has been summed up to the Si^{4+} measured in solution and plotted as rescaled Si^{4+}. Hence, Fig. 1

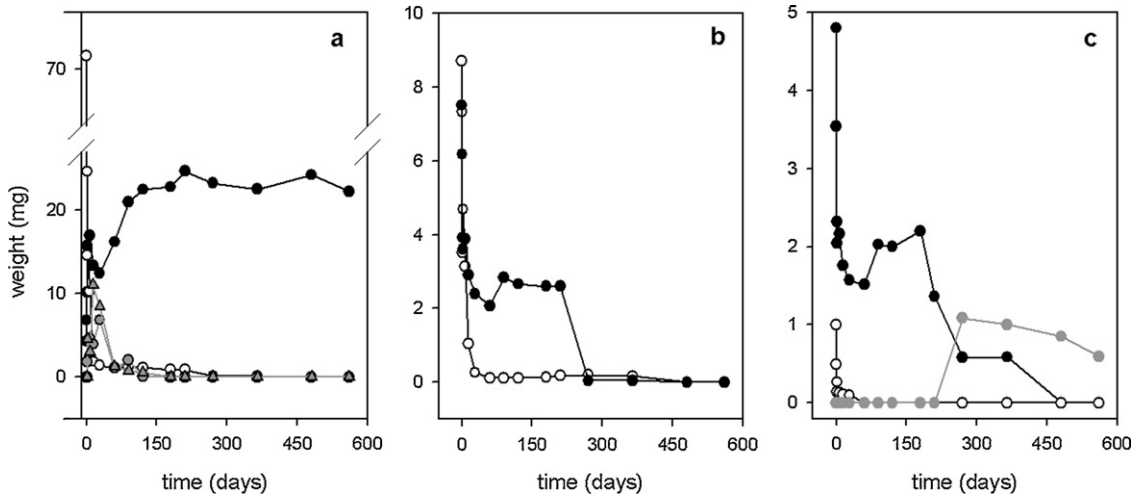

Fig. 3. Evolution of the crystalline phases contained in KRY·AS (line 1, Sample 1) during the dissolution experiment. Legend: (a) Black dots = amorphous phase; empty dots = β-larnite (C2S); grey triangles = calcite ($CaCO_3$); grey dots = portlandite ($Ca(OH)_2$). (b) Black dots = merwinite ($Ca_3MgSi_2O_8$); empty dots = periclase (MgO). (c) Black dots = ferrite (C4AF); empty dots = akermanite ($Ca_2MgSi_2O_7$); grey dots = hematite (α-Fe_2O_3).

also reports the amount of SiO_2 corresponding to the amount of Si^{4+} effectively dissolved and eventually precipitated back from the solution. If we sum the latter to the calculated raw weight loss (black dots in Fig. 1), we obtain the actual weight loss during KRY·AS dissolution (grey dots in Fig. 1). Hence, 100% of the raw weight loss is never achieved not because of incomplete dissolution of KRY·AS but because silica is precipitated back from the solution and its weight sum up to the residual KRY·AS fraction.

The concentration of magnesium released in solution with time (Fig. 2) and the evolution of the Mg-bearing crystalline phases (Fig. 3) reveals that most of the magnesium ions are released within the first 60 days in correspondence with the dissolution of periclase (empty circles in Fig. 3b). A further minor release in the range 90–250 days is due to the dissolution of merwinite (black dots in Fig. 3b).

The trend of Al^{3+} release (Fig. 2) compared to the evolution of Al-bearing crystalline phases (Fig. 3c) indicates that the crystalline phase responsible for the release of Al^{3+} in solution is ferrite (C4AF, $4CaO{\cdot}Al_2O_3{\cdot}Fe_2O_3$). As a matter of fact, ferrite starts to dissolve after 200 days and is the last crystalline phase to disappear, after *ca.* 350–400 days, when pH < 5.0 and Fe^{3+} becomes soluble [30]. It is possible that some aluminium is also released after merwinite dissolution as, according to Larsen and Foshag [31], Al^{3+} can be found in the tetrahedral sites of merwinite. The release of Al^{3+} in solution becomes significant only after *ca.* 200 days when the pH of the solution is close to 4. The release of iron in solution occurs only after *ca.* 270 days (Fig. 2) when pH is well below 4.5. Fe^{3+} is released by the dissolving ferrite (C4AF) phase (black dots in Fig. 3c). In correspondence with the release of iron in solution, hematite formation is detected in the residue (grey dots in Fig. 3).

The presence of hematite has been confirmed in the KRY·AS system with powder diffraction and micro-Raman as already reported in [32].

This secondary phase is the only crystalline phase found in KRY·AS at the end of the experiment and, together with precipitated silica, contributes to the residual fraction (Fig. 1). Because hematite is amphoteric and dissolves in acid media [33], it should not be stable in our systems and must have formed during the calcinations process to obtain the KRY·AS residue.

3.2. Dissolution in organic simulated lung fluids

In the second experimental line, since the starting modified Gamble solution was buffered, pH values were stable and rarely exceeded 5.0. In general, a comparison with the results obtained from the first experimental line shows that the dissolution rates of the second line are much higher (see Fig. 4 and Supplementary data Table S3), so that after about 13 days the KRY·AS samples have already reached their maximum value of weight loss (*ca.* 88 wt%).

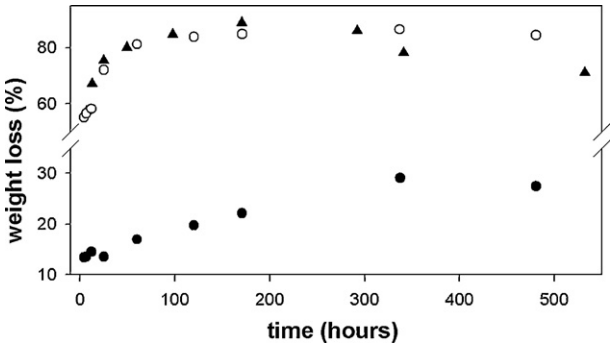

Fig. 4. Evolution of pH of the suspension and weight of the residual fraction of KRY·AS with time (experimental line 2). Legend: empty dots = KRY·AS Sample 2; black triangles = KRY·AS Sample 3; black dots = standard chrysotile asbestos (Sample 4).

Absolute concentrations of the elements as detected in solution at different times are summarized in Fig. 5 and Supplementary data Table S4. Silicon is brought into solution very quickly in both Samples 2 and 3, with a higher dissolution rate for the latter. In both samples, magnesium reaches a plateau just after 48 h, with different absolute values reflecting the different Mg^{2+} content of the two samples (Table 1). In chrysotile, Si^{4+} and Mg^{2+} show a trend in accordance with the overall weight loss of this sample. Calcium is released in solution in about 120 days for Sample 2 and 100 days for Sample 3, respectively followed by a slight decrease that is due to precipitation of Ca-bearing phases during the final stages of the experiment. Release of aluminium and iron is strictly dependent upon their narrow solubility field. A pH of 4.5 falls in a region where their solubility is very low [34]. As a consequence, measured concentrations for most replicates are under the instrumental detection limit (see Supplementary data Table S4). Under these conditions no clear trends were recognizable.

The SEM investigation (Supplementary data Figs. S3a and S3b for Samples 2 and 3, respectively) evidences for both samples the tendency to decrease the crystal size with time, and the gradual appearance of halite (NaCl), whitlockite

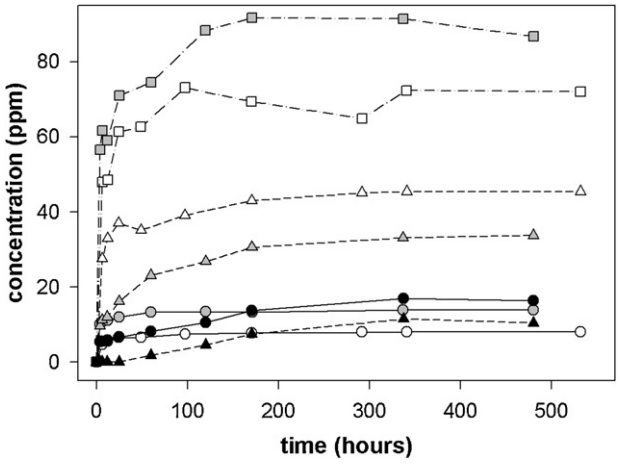

Fig. 5. Release in solution of the major elements contained in KRY·AS (Samples 2 and 3) and standard chrysotile asbestos (experimental line 2) during the dissolution experiment. Legend: grey dots = Sample 2, Mg^{2+}; grey squares = Sample 2, Ca^{2+}; grey triangles = Sample 2, Si^{4+}; empty dots = Sample 3, Mg^{2+}; empty squares = Sample 3, Ca^{2+}; empty triangles = Sample 3, Si^{4+}; black dots = Sample 4, Mg^{2+}; black triangles = Sample 4, Si^{4+}.

($Ca_9(Mg,Fe)(PO_4)_6(PO_3OH)$), tychite ($Na_6Mg_2(CO_3)_4(SO_4)$) and tridymite ($SiO_2$) after about 170 h. Halite, a component of the Gamble solution, is often found in small crystals finely dispersed throughout the residue. After 4 h, residual crystals are still visible but later their dimensions are progressively reduced. Towards the end of the experiment, ferrite is also observed. Akermanite and C2S crystals are found in the sample replicates taken after 6.5 h and after 24.5 h. At later times they became quite rare. An exception is the akermanite/gehlenite individual found after 170.5 h. At longer dissolution times, the presence of newly formed phases is detected (*i.e.* whitlockite at 532 h).

Fig. 6 reports the absolute weight of crystalline phases *vs.* time. In accordance with the total weight loss, the general trend is to bring absolute weights close to zero in less than 300 h.

C2S quickly dissolves during the first 12 h for Samples 2 and 3. The same occurs for akermanite, merwinite and bredigite, for Sample 3, and periclase and portlandite for Sample 2. The dissolution of these phases is accompanied by massive release of Ca^{2+}, Mg^{2+} and Si^{4+} in solution (see Fig. 5). Lower dissolution rates are found for wollastonite (Fig. 6h), quartz (Fig. 6g) and ferrite (Fig. 6a). For both samples, the sum of amorphous fraction and newly formed phases shows a complex trend. Because its original amorphous content is relatively small, the dominant effect in the first 6 h in Sample2 is the dissolution of crystalline phases prompting a remarkable increase of the amorphous content (see Fig. 6a). After 24 h, when this contribution is reduced, the amorphous fraction follows a depletion trend. Later, a plateau is reached, and, as precipitation of new phases dominates, a new increase occurs towards the end of the experiment for the precipitation of secondary silica. The amorphous content of Sample 3, as reported in Table 1, is more than twice as large as that of Sample 2. The effect of its dissolution will consequently be higher. Actually, as evidenced in Fig. 6e, in the first period (6 h), the amorphous contribution is dominant. This contribution is still dominant after 12 h, as crystalline phase dissolution is almost exhausted. During the second part of the experiment, the precipitation of new phases counterbalances this trend.

In Samples 2 and 3, increasing amounts of halite were detected after 120 h and 171 h, respectively. Halite is later substituted by whitlockite and tychite (292 h). In both Samples 2 and 3, secondary silica appeared after 340 h as trydimite, plausibly crystallized during the sample heating in the platinum crucible (see Section 2.3) from the amorphous Si-rich phase provided by the dissolution of silicates. As depicted in Fig. 6g, the presence of silica in solution may also originate from the dissolution of quartz, that has been detected only in Sample 3. Its smooth decrease, evidenced in Fig. 6g, and the absence of any appreciable variation in the shape of the (1 0 1) diffraction reflection, suggest that a re-precipitation of silica as quartz can be excluded. C4AF and magnetite, detected in Samples 2 and 3, respectively (Fig. 6a and g), are the main iron bearing phases. As already discussed, ferrite dissolves very slowly. Iron released after phase dissolution has been detected in the residue as hematite starting from 170 h to the end of the experiment. Hematite should have formed similarly to what was already described in Section 3.1.

3.3. Dissolution in inorganic vs. organic simulated lung fluids

A comparison of the results of our dissolution experiments conducted with inorganic and organic simulated lung fluids clearly shows that the contour experimental conditions play a key role and totally different dissolution rates may be obtained if such conditions are varied. It is clear from the kinetics of the dissolution process that the rate determined from experimental line 1 is far slower than the dissolution rate determined from experimental line 2 (dissolution time of 253 days for experimental lines 1 and 20 days for experimental line 2, respectively in Table 2). Comparable estimated times of dissolution of chrysotile from experimental line 2 and from the experiment described in [17] with inorganic dilute HCl solution, indicate that the nature of the solution used is probably not a major factor governing the rate of dissolution of the investigated materials. It was also demonstrated that the rates at 25 °C and at 37 °C determined for the experimental line 1 are nearly identical (Supplementary data Fig. S1) indicating that the rates of reaction kinetics are comparable at these two temperatures. As far as the buffering condition is concerned, Christensen et al. [35] have demonstrated that the dissolution rates for different Ca–Si-rich man-made vitreous fibres in a dynamic flow-through method experiment and in a stationary experiment (where pH was manually adjusted just like the one conducted here) were in the same relative order. This seems to downgrade the importance of buffering as the dissolution rate limiting factor. Minor influence of the different agitation conditions is also expected because even in [17] the suspension is apparently not agitated. Besides that, the bottles in experimental line 1 were shaken every day simulating some sort of agitation. Thus, the major factor which should govern the different rate of dissolution in the two experimental line is the early saturation of silica due to the high solidus/liquidus ratio. Oze and Solt [22] have already demonstrated that in undersaturation region, the rate of Si^{4+} release is influenced by the concentration of particles in suspension. The high suspension density in the experimental line 1 prompts an early saturation of the system with respect to silicon and a limitation of the dissolution speed of the overall system. As a matter of fact, our experimental results show that KRY·AS (with 1–2 m^2/g specific area: see Table 1) prompts silica saturation when solidus/liquidus (mg/ml) = 0.67 whereas saturation does not occur when the ratio is 0.2. Comparable results have been obtained for chrysotile (with 6.14 m^2/g specific area) suspension in a simulated gastric fluid SGF solution (pH 1.2) where silica saturation of the solution is attained with large solidus/liquidus ratios whereas no saturation is observed when the ratio is 0.2 [22]. Although many factors such as chemistry and specific surface of the solid phase and pH of the solution, affect silica saturation of the solution in these systems, saturation in general is certainly prevented when solidus/liquidus (mg/ml) is set to very low values (<0.2).

Hence, the low dissolution rate of silica in acid solution (well described in the literature [36]) is the actual rate limiting step of the overall dissolution kinetic. Moreover, it is well known that the lifetime of chrysotile fibres is controlled by the dissolution rate

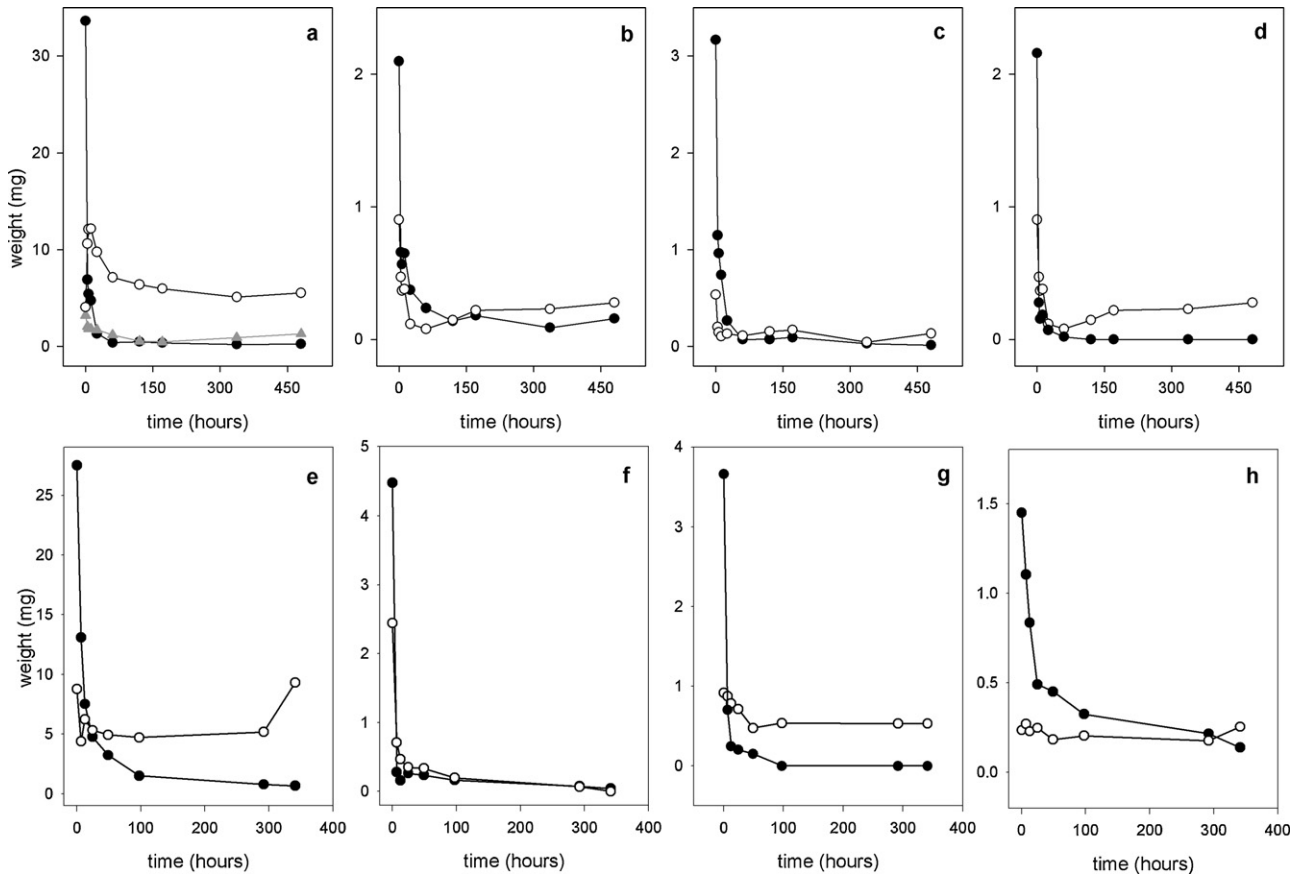

Fig. 6. Evolution of the crystalline phases contained in KRY·AS (line 2, Samples 2 and3) during the dissolution experiment. Legend: Sample 2 (a) empty dots = amorphous phase; black dots = β-larnite (C2S); grey triangles = ferrite (C4AF). (b) Empty dots = merwinite ($Ca_3MgSi_2O_8$); black dots = portlandite ($Ca(OH)_2$). (c) Empty dots = wollastonite ($CaSiO_3$); black dots = periclase (MgO). (d) Empty dots = yeelimite ($Ca_4Al_6O_{12}(SO_4)$); black dots = ternesite (silicocarnotite $Ca_5(SiO_4)_2SO_4$). Sample 3: (e) empty dots = amorphous phase; black dots = akermanite ($Ca_2MgSi_2O_7$). (f) Empty dots = β-larnite (C2S); black dots = merwinite ($Ca_3MgSi_2O_8$). (g) Empty dots = quartz (α-SiO_2); black dots = bredigite ($Ca_7Mg(SiO_4)_4$). (h) Empty dots = magnetite (α-Fe_3O_4); black dots = wollastonite ($CaSiO_3$).

of the silica layer as magnesium in acidic environment quickly leaches [17,37]. This also applies to the Ca–Mg–Si-rich cement phases contained in KRY·AS whose behaviour resemble that of common Portland cement phases (see Section 3.1) with the silicate and aluminate phases decomposed with removal of calcium [38].

3.4. Kinetic analysis

The kinetic analysis of the dissolution of KRY·AS cannot be undertaken using the same approaches described for single mineral phases (chrysotile and tremolite) in the literature [17,22].

Table 2
Comparison of dissolution times in acid environment of the main natural and man-made mineral/vitreous fibres (MMMF/MMVF).

Phase	pH of the solution	Mean particle diameter D_0 or $D_0 \times L$ (length) (μm)	Estimated dissolution time (days)[a]	Mode of the experiment and solidus/liquidus ratio (mg/ml)	Reference
Amosite	4.5	0.5	2500[b]	Dynamic	[45]
Amorphous silica	2.0–6.0	1.0	159,870	Static 0.1	[44]
KRY·AS sample 1	4.5	10.0	253(15)	Static 0.67	This study
KRY·AS sample 2	4.5	10.0	20(1)	Static 0.2	This study
KRY·AS sample 3	4.5	7.0	20(1)	Static 0.2	This study
Chrysotile	4.0	1.0 × 10.0	180	Dynamic	[45]
Chrysotile	2.0–6.0	1.0 × 10.0	270	Not reported	[17]
Chrysotile	1.2	<10.0	1	Static 0.5–50	[22]
Chrysotile NIST	4.5	1.0 × 10.0	298(18)	Static 0.2	This study
Crocidolite	4.5	0.5	5000[b]	Dynamic	[45]
MMMF ceramic fibres	4.5	1.54	350[b]	Dynamic	[45]
MMVF glass wool	4.5	1.44	277[b]	Dynamic	[45]
MMVF glass wool	4.5	1.14	1900[b]	Dynamic	[45]
MMVF rock wool	4.5	1.43	178[b]	Dynamic	[45]
MMVF slag wool	4.5	1.41	47[b]	Dynamic	[45]
Tremolite	1.2	<10.0	274	Static 0.5–50	[22]
Quartz	2.0–6.0	1.0	6.2×10^8	Static 0.1	[44]

[a] Estimated error in parenthesis.
[b] Calculated from the equation: $t = D_0/2\nu_{Si}$ using the rate constants for the dissolution of Si ν_{Si} from Table 4 after [58].

KRY·AS is a polyphasic system and therefore, following the kinetics of dissolution reaction of a single element such as silicon and/or magnesium may not be indicative of the overall reaction kinetics. In the case of chrysotile, because the dissolution reaction for pH < 9.0 is $Mg_3(OH)_4Si_2O_5 + 6H^+ = 3Mg^{2+} + 2H_4SiO_4 + H_2O$, Hume and Rimstidt [17] followed the reaction kinetics by monitoring the dissolution of silicon and magnesium and applying a shrinking particle model. Even the dissolution process of cement and carbonate systems in acid environment is followed by monitoring specific chemical parameters as the release of calcium in solution [39]. For calcite and dolomite at pH values above approximately 4.0 the surface reactions dominate. The surface area normalized dissolution rate is given by $r = k_a c_H{}^n$ where c_H is the proton concentration adjacent to the mineral surface and k_a the rate constant. The exponent n is the order of the reaction.

In this study to follow the overall dissolution reaction of KRY·AS and determine the relative kinetic parameters, the analysis has been performed using a direct evidence of the dissolution process, the actual (residual) weight *vs.* time. The rescaled residual weight has been converted into the conversion factor (α: [40]) to draw the α-time plot (Fig. 7a) to be treated as a conventional isothermal curves at 37 °C. For the isothermal analysis, the following general kinetic equation in the integral form can be used: $g(\alpha) = kt$ [41,42]. An appropriate kinetic model function $g(\alpha)$ is usually estimated by plotting $g(\alpha)$ *vs.* t with the rate constant k calculated from the slope of the line obtained. For all the experiments, the best fit (Fig. 7b) was obtained with an F3 third order reaction model, an appropriate approximation to describe solution mediated reactions [43]. The regression coefficients are $0.9867 \leq R^2 \leq 0.9974$ and the calculated rate constants are $k = 7.978 \times 10^{-6}\ min^{-1}$ for standard chrysotile; $k = 8.410 \times 10^{-4}\ min^{-1}$ for KRY·AS Sample 1; $k = 7.346 \times 10^{-3}\ min^{-1}$ for KRY·AS Sample 2; $k = 7.445 \times 10^{-3}\ min^{-1}$ for KRY·AS Sample 3. The sigmoid kinetic equation used for the determination of the rate constants cannot be used for the determination of the total dissolution times of the investigated samples because for $\alpha \to 1$, time $(t) \to$ +infinite. To do this, a fit with an empirical nonlinear expression was used. The best fit was obtained using the equation $\alpha = \alpha_0 + a \times \ln(t - t_0)$ which allowed the determination of the parameters α_0, a, and t_0. The regression coefficients are $0.9919 \leq R^2 \leq 0.9991$. The total dissolution times was then determined by simply make α equal to 1 in the expression $\alpha = \alpha_0 + a \times \ln(t - t_0)$ to get:

$$t = \frac{\exp[1 - \alpha_0/a]}{t_0}$$

The values are reported in Table 2 together with dissolution times from the existing literature known to the authors for the *in vitro* dissolution of various mineral particles, natural and man-made mineral fibres. The estimated dissolution time of KRY·AS is fairly shorter with respect to the chrysotile standard used for comparison and with respect to minerals such as amosite, crocidolite, and quartz considered carcinogenic by the International Agency for Research on Cancer. Tremolite displays shorter dissolution time but it was dissolved in a strongly acid solution (pH 1.2). The slow dissolution rate of KRY·AS Sample 1 in inorganic solution is due to the formation of amorphous silica. The formation of amorphous silica and its role as rate limiting step of the dissolution reaction has already been pointed out in [17] and witnessed by its extremely sluggish dissolution time. It is true that organic compounds that complex and make silica soluble will likely shorten the life-time of a fibre (particle), whereas compounds that adsorb and protect it from dissolution will increase the lifetime of the fibre (particle) [17].

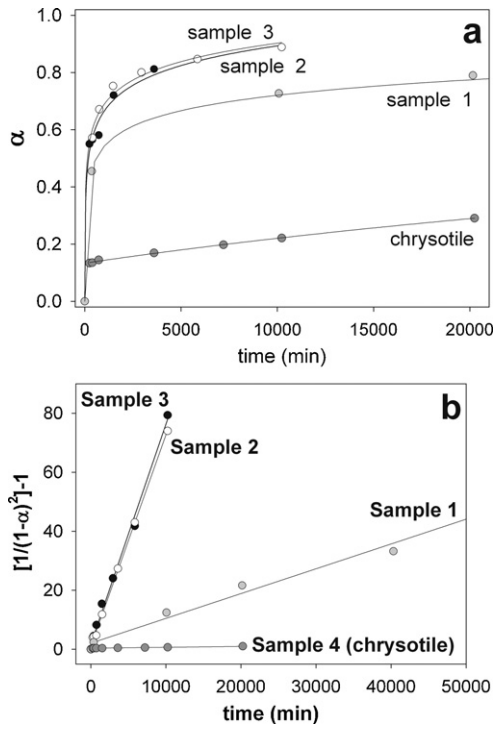

Fig. 7. (a) The α-time plots relative to the dissolution kinetics of the investigated samples. (b). The best fit obtained using an F3 kinetic equation relative to the kinetic analysis of the curves plotted in (a), see the text for details.

4. Conclusions

In vitro biodurability was tested on the products of transformation of cement–asbestos at 1200 °C (KRY·AS) using both inorganic and organic simulated lung fluid. It was proven that the experimental conditions strongly influence the rate of dissolution and the total dissolution time. The latter was estimated from the experimental line using inorganic HCl diluted solution without buffering to be of an order of magnitude higher than that determined from buffered Gamble solution (253 days *vs.* 20 days). Equally to chrysotile asbestos, the rate limiting step of the overall dissolution reaction is the dissolution of silica as its solubility in acid environment (macrophage intracellular environment) is very low. The calculation of the rate constants of dissolution reveal that, in agreement with literature data, standard chrysotile asbestos dissolves very slowly at pH 4.5 with respect to KRY·AS. Therefore, the biodurability *in vitro* of KRY·AS is much lower with respect to that of chrysotile asbestos (total estimated dissolution time of 20 days *vs.* 298 days, respectively). This is a further verification of the very low potential toxicity of this secondary raw material. These results are of great importance because they are a further confirmation of the viability of the process of thermal transformation of cement–asbestos into a secondary raw material to be safely recycled in different industrial applications.

Acknowledgments

ZETADI s.r.l. is acknowledged for granting this project within a long term cooperation agreement with the Earth Sciences Dept., The University of Modena and Reggio Emilia, Italy. Thanks to the technical staff of the C.I.G.S. Laboratory (The University of Modena and R.E.) and especially G. Urso and M. Tonelli for help during the SEM a experimental sessions. We kindly acknowledge Dr. M. Lassinantti Gualtieri for fruitful discussions and careful reading of the manuscript. Thanks to T. Giliberti, now retired, for her help with the lab dissolution experiments. We finally would like to thank the

two anonymous referees for their careful revision and constructive suggestions which greatly improved the quality of the manuscript.

Appendix A. Supplementary data

Supplementary data associated with this article can be found, in the online version, at doi:10.1016/j.jhazmat.2011.12.005.

References

[1] S.P. Johnson, G. Corcelle, The Environmental Policy of the European Communities, second ed., International Environmental Law and Policy Series, Kluver Law International, London, 1995, p. 515.
[2] B.R. Babic, The use of cement fibre composites in prolonged wet environments, in: 10th International Inorganic-Bonded Fiber Composites Conference, Curran Associates, São Paulo, 2006, pp. 260–273.
[3] C.M.R. Dias, M.A. Cincotto, H. Savastano Jr., V.M. John, Long-term aging of fiber–cement corrugated sheets – the effect of carbonation, leaching and acid rain, Cement Concrete Compos. 30 (2008) 255–265.
[4] C. Abruzzese, A.M. Marabini, F. Paglietti, P. Plescia, in: B. Mishra (Ed.), CORDIAM Process: A New Treatment for Asbestos Wastes, Congress Book, 1998, pp. 563–577.
[5] A. Borderes, Vitrification of the incineration residues, Rev. Verre 6 (4) (2000) 1–2.
[6] A. Downey, D.M. Timmons, Study into the applicability of thermochemical conversion technology to legacy asbestos wastes in the UK, in: WM'05 Abstract Conference Book, February 27–March 3, 2005, Tucson, AZ, USA, 2005.
[7] C. Leonelli, P. Veronesi, D.N. Boccaccini, M.R. Rivasi, L. Barbieri, F. Andreola, I. Lancellotti, D. Rabitti, G.C. Pellacani, Microwave thermal inertisation of asbestos containing waste and its recycling in traditional ceramics, J. Hazard. Mater. B 35 (2006) 149–155.
[8] F. Dellisanti, P.L. Rossi, G. Valdrè, Remediation of asbestos containing materials by Joule heating vitrification performer in a pre-pilot apparatus, Int. J. Miner. Process. 91 (2009) 61–67.
[9] T. Zaremba, A. Krzakała, J. Piotrowski, D. Garczorz, Study on the thermal decomposition of chrysotile asbestos, J. Therm. Anal. Calorimet. 101 (2010) 479–485.
[10] K. Anastasiadou, D. Axiotis, E. Gidarakos, Hydrothermal conversion of chrysotile asbestos using near supercritical conditions, J. Hazard. Mater. 179 (2010) 926–932.
[11] A.F. Gualtieri, C. Cavenati, I. Zanatto, M. Meloni, G. Elmi, M. Lassinantti Gualtieri, The transformation sequence of cement–asbestos slates up to 1200 °C and safe recycling of the reaction product in stoneware tile mixtures, J. Hazard. Mater. 152 (2008) 563–570.
[12] A. Cattaneo, A.F. Gualtieri, G. Artioli, Kinetic study of the dehydroxylation of chrysotile asbestos with temperature by in situ XRPD, Phys. Chem. Miner. 30 (2001) 177–183.
[13] A.F. Gualtieri, D. Levy, E. Belluso, M. Dapiaggi, Kinetics of the decomposition of crocidolite asbestos: a preliminary real-time X-ray powder diffraction study, Mater. Sci. Forum 443–444 (2004) 291–294.
[14] A.F. Gualtieri, C. Giacobbe, L. Sardisco, M. Saraceno, M. Lassinantti Gualtieri, G. Lusvardi, C. Cavenati, I. Zanatto, Recycling of the product of thermal inertization of cement–asbestos for various industrial applications, Waste Manage. 31 (2011) 91–100.
[15] G. Oberdörster, Determinants of the pathogenicity of man-made vitrosu fibers (MMVF), Int. Arch. Occup. Environ. Health 73 (2000) 560–568.
[16] F. Giantomassi, A.F. Gualtieri, L. Santarelli, M. Tomasetti, G. Lusvardi, G. Lucarini, M. Governa, A. Pugnaloni, Biological effects and comparative cytotoxicity of thermal transformed asbestos-containing materials in a human alveolar epithelial cell line, Toxicol. In Vitro 24 (6) (2010) 1521–1531.
[17] A. Hume, J.D. Rimstidt, The biodurability of chrysotile asbestos, Am. Mineral. 77 (1992) 1125–1128.
[18] J.M.G. Davis, The biological effects of mineral fibres, Ann. Occup. Hyg. 24 (1981) 227–234.
[19] D.M. Bernstein, R. Rogers, P. Smith, The biopersistence of Brazilian chrysotile asbestos following inhalation, Inhal. Toxicol. 17 (11–12) (2004) 745–761.
[20] D.M. Bernstein, J. Chevalier, P. Smith, Comparison of Calidria chrysotile asbestos to pure tremolite: final results of the inhalation biopersistence and histopathology examination following short-term exposure, Inhal. Toxicol. 17 (2005) 427–449.
[21] D.M. Bernstein, K. Donaldson, U. Decker, S. Gaering, P. Kunzendorf, J. Chevalier, S.E. Holm, A biopersistence study following exposure to chrysotile asbestos alone or in combination with fine particles, Inhal. Toxicol. 20 (11) (2008) 1009–1028.
[22] C. Oze, K. Solt, Biodurability of chrysotile and tremolite asbestos in simulated lung and gastric fluids, Am. Mineral. 95 (2010) 825–883.
[23] A. de Meringo, C. Morsscheidt, S. Thélohan, H. Tiesler, *In vitro* assessment of biodurability: acellular systems, Environ. Health Perspect. 102 (1994) 47–53.
[24] R. Laviano, M. Moresi, D. Perniola, F. Balenano, Materiali contenenti amianto in matrice cementizia:possibile riutilizzo quale materia prima-seconda nella realizzazione di laterizi, Atti del Convegno L'industria e l'amianto–i nuovi materiali e le nuove tecnologie a dieci anni dalla Legge 257/1992, Roma 26–28 novembre 2002 (in Italian).
[25] H.M. Rietveld, A profile refinement method for nuclear and magnetic structures, J. Appl. Crystallogr. 2 (1969) 65–71.
[26] A.C. Larson, R.B. Von Dreele, Generalized Structure Analysis System, LosAlamos Nat. Lab., New Mexico, LAUR, 1999, pp. 86–748.
[27] B.H. Toby, EXPGUI, a graphical user interface for GSAS, J. Appl. Crystallogr. 34 (2001) 210–213.
[28] A.F. Gualtieri, Accuracy of XRPD QPA using the combined Rietveld–RIR method, J. Appl. Crystallogr. 33 (2000) 267–278.
[29] S. Chatterji, Mechanism of the $CaCl_2$ attack on Portland cement concrete, Cement Concrete Res. 8 (1978) 461–468.
[30] V. Chevrier, F. Poulet, J.P. Bibring, Early geochemical environment of Mars as determined from thermodynamics of phyllosilicates, Nature 448 (2007) 60–63.
[31] E.S. Larsen, W.F. Foshag, Merwinite, a new calcium magnesium orthosilicate from Crestmore, California, Am. Mineral. 6 (1921) 143–148.
[32] C. Giacobbe, A.F. Gualtieri, S. Quartieri, C. Rinaudo, M. Allegrina, G.B. Andreozzi, Spectroscopic study of the product of thermal transformation of chrysotile-asbestos containing materials (ACM), Eur. J. Mineral. 22 (2010) 535–546.
[33] R.M. Cornell, U. Schwertmann, The Iron Oxides. Structure, Properties, Reactions, Occurrence and Uses, Wiley-VCH, Weinheim, 2003, p. 661.
[34] B. Mason, Principles of Geochemistry, John Wiley and Sons, 1966, p. 274.
[35] V.R. Christensen, S. Lund Jensen, M. Guldberg, O. Kamstrup, Effect of chemical composition of man-made vitreous fibres on the rate of dissolution *in vitro* at different pHs, Environ. Health Perspect. 102 (5) (1998) 83–86.
[36] R.K. Iler, The Chemistry of Silica, Wiley Interscience Publication, New York, 1979, p. 866.
[37] A. Morgan, P. Davies, J.C. Wagner, G. Berry, A. Holmes, The biological effects of magnesium- etched chrysotile asbestos, Brit. J. Exp. Pathol. 58 (1977) 465–473.
[38] H.F.W. Taylor, Cement Chemistry, Academic Press, 1997.
[39] J.W. Morse, R.S. Arvidson, The dissolution kinetics of major sedimentary carbonate minerals, Earth Sci. Rev. 58 (2002) 51–84.
[40] A.K. Galway, M.E. Brown, Thermal Decomposition of Ionic Solids: Chemical Properties and Reactivities of Ionic Crystalline Phases, Elsevier, 1999, p. 597.
[41] H. Tanaka, Thermal analysis and kinetics of solid state reactions, Thermochim. Acta 267 (1995) 29–44.
[42] C.H. Bamford, C.H.F. Tipper, Comprehensive Chemical Kinetics, vol. 22, Elsevier, New York, 1980, pp. 41–113.
[43] M.J. Pilling, P.W. Seakins, Reaction Kinetics, Oxford Science Publications, Oxford, 1995, p. 305.
[44] J.D. Rimstidt, H.L. Bames, The kinetics of silica–water reactions, Geochim. Cosmochim. Acta 44 (1980) 1683–1699.
[45] M. Guldberg, V.R. Christensen, M. Perander, B. Zoitos, A.R. Koenig, K. Sebastian, Measurement of in vitro fibre dissolution rate at acidic pH, Ann. Occup. Hyg. 42 (1998) 233–243.